8-27-2021

High Depth-of-Discharge Zinc Rechargeability Enabled by a Self-Assembled Polymeric Coating

David J. Arnot
Sandia National Laboratories

Matthew B. Lim
Sandia National Laboratories

Nelson S. Bell
Sandia National Laboratories

Noah B. Schorr
Sandia National Laboratories

Ryan C. Hill
University of Kentucky, Ryan.C.Hill@uky.edu

See next page for additional authors

Repository Citation

High Depth-of-Discharge Zinc Rechargeability Enabled by a Self-Assembled Polymeric Coating

Notes/Citation Information

Authors

David J. Arnot, Matthew B. Lim, Nelson S. Bell, Noah B. Schorr, Ryan C. Hill, Andrew Meyer, Yang-Tse Cheng, and Timothy N. Lambert

High Depth-of-Discharge Zinc Rechargeability Enabled by a Self-Assembled Polymeric Coating

David J. Arnot, Matthew B. Lim, Nelson S. Bell, Noah B. Schorr, Ryan C. Hill, Andrew Meyer, Yang-Tse Cheng, and Timothy N. Lambert*

Zinc has the potential for widespread use as an environmentally friendly and cost-effective anode material pending the resolution of rechargeability issues caused by active material loss and shape change. Here, a self-assembled Nafion-coated Celgard 3501 (NC-Celgard) separator is shown to enable unprecedented cycle life of a Zn anode in alkaline electrolyte at high depth-of-discharge (DOD_{Zn}). Using commercially relevant energy-dense electrodes with high areal capacities of 60 mAh cm^{-2}, Zn–Ni cells tested at 20% DOD_{Zn} cells achieve over 200 cycles while 50% DOD_{Zn} cells achieve over 100 cycles before failure. The 20% and 50% DOD cells deliver an average of 132 and 180 Wh L^{-1} per cycle over their lifetime respectively. Rechargeability is attributed to the highly selective diffusion properties of the 300 nm thick negatively charged Nafion coating on the separator which prevents shorting by dendrites and inhibits redistribution of the active material. Crossover experiments show that the NC-Celgard separator is practically impermeable to zincate ($[Zn(OH)_4]^{2-}$), outperforming commercial Celgard, cellophane, Nafion 211 and 212 separators while still allowing hydroxide transport. This work demonstrates the efficacy of selective separators for increasing the cycle life of energy-dense Zn electrodes without adding significant volume or complexity to the system.

1. Introduction

Batteries utilizing a Zn anode and aqueous alkaline electrolyte are a desirable alternative to lithium-ion batteries which have intrinsic issues associated with safety, cost, and material abundance.[1–3] In addition to a high specific capacity (820 mAh g^{-1}) and low redox potential (−0.762 V vs SHE), Zn has the advantages of being environmentally benign, low-cost, and earth abundant.[4] Paired with a MnO_2, Ag_2O, NiOOH, CuO, or air cathode, Zn-based batteries are capable of high specific energy densities up to 500 Wh kg^{-1}.[5–7] Additionally, recent reports of dual-electrolyte systems have shown the feasibility of high-voltage (>2 V) Zn batteries.[8–10]

Despite some notable advances in the field, Zn electrodes have generally not demonstrated long cycle lifetime at high depth-of-discharge (DOD_{Zn}) in alkaline electrolyte. The formation of dendrites, passivation from ZnO, and active material redistribution (shape change) are the main problems limiting the performance of Zn as an anode in secondary alkaline batteries.[11] The high solubility of ZnO in alkaline electrolyte [as zincate, $Zn(OH_4)^{2-}$] causes shape change and dendrite formation as dissolved species are plated out of solution away from their original location due to uneven current distribution. Several strategies have been employed to circumvent these issues, including encapsulation of the Zn (or ZnO) particles,[12–16] additives,[17] new electrode geometries,[4,18] and separators.[19–25] Selective separators have the potential to improve Zn anode rechargeability by limiting the migration of Zn into the bulk electrolyte, impeding active material loss and shape change, and preventing shorting by Zn dendrites.[26]

2. Results and Discussion

Following on previous work incorporating Nafion into aqueous Zn batteries,[9,17,23,27] we characterize the performance and physical properties of a commercial polypropylene separator (Celgard 3501) modified by a thin self-assembled Nafion coating in an alkaline Zn–Ni battery. The Nafion-coated Celgard (NC-Celgard) separators were prepared by a simple dip coating procedure where Celgard was soaked in a 5.0% Nafion dispersion for 20 h and dried in ambient air (**Figure 1**a; Figure S1, Supporting

D. J. Arnot, M. B. Lim, N. B. Schorr, T. N. Lambert
Department of Photovoltaics and Materials
Sandia National Laboratories
Albuquerque, NM 87185-0734, USA
E-mail: tnlambe@sandia.gov

M. B. Lim
Department of Energy Storage Technology and Systems
Sandia National Laboratories
Albuquerque, NM 87185-0734, USA

N. S. Bell
Advanced Materials Laboratory
Sandia National Laboratories
Albuquerque, NM 87185-0734, USA

R. C. Hill, A. Meyer, Y.-T. Cheng
Department of Chemical and Materials Engineering
University of Kentucky
Lexington, KY 40506, USA

ADVANCED
SCIENCE NEWS
www.advancedsciencenews.com

ADVANCED
ENERGY
MATERIALS
www.advenergymat.de

Figure 1. a) Preparation of NC-Celgard by submersion of Celgard 3501 in 5.0% Nafion solution for 20 h and air drying at RT. SEM images of b) Celgard 3501 as received and c) NC-Celgard. d) FTIR spectrum for unmodified Celgard 3501 and NC-Celgard with peaks at 1150 and 1204 cm⁻¹ indicating C–F bond stretching. e) Cross-sectional SEM image of NC-Celgard showing a coating thickness of about 300 nm and f) the EDS map confirming the Nafion coating with fluorine content only on the surface of the separator.
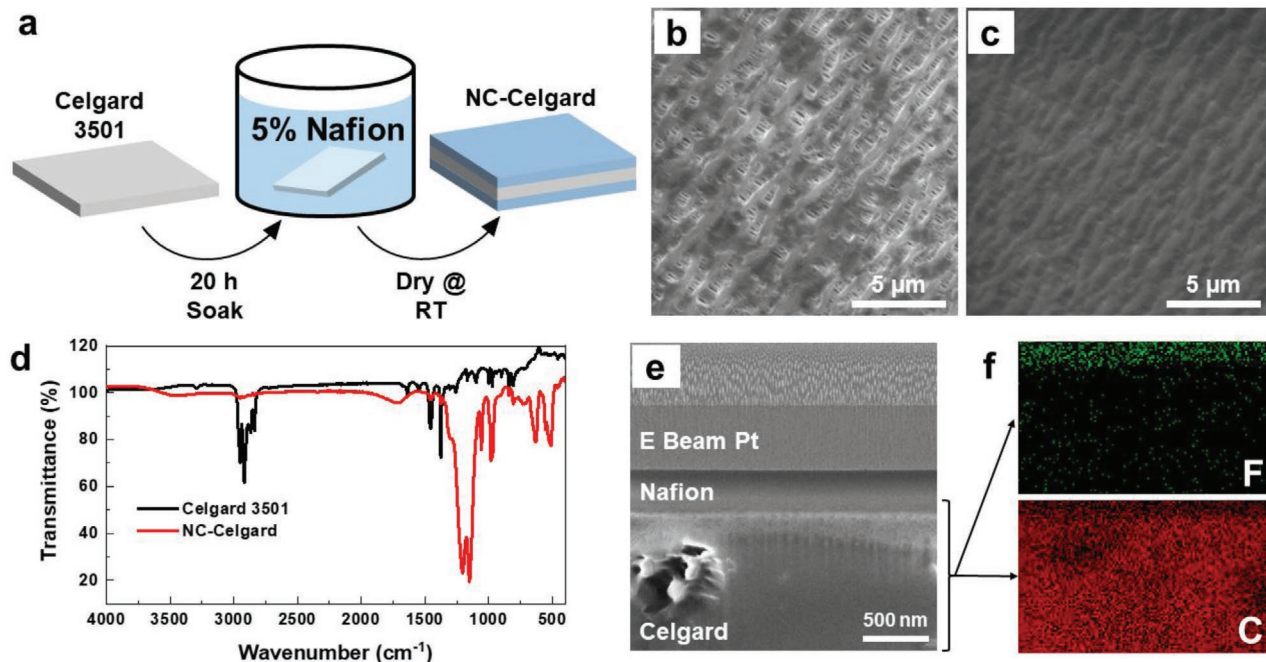
Information). Scanning electron microscopy (SEM) images before and after soaking show that a dense layer of Nafion is deposited onto the polypropylene, covering the pore structures (Figure 1b,c). The Nafion coating has a mass loading of ≈ 0.28 mg cm^{-2}. Nafion dispersions of 1.0% and 2.5% were also tested to investigate the effect of concentration on coating thickness, but these lower concentrations did not produce consistent coverage (Figure S2, Supporting Information). Energy-dispersive X-ray spectroscopy (EDS) and Fourier transform infrared spectroscopy (FTIR) were used to further characterize the structure. The EDS spectrum of the Nafion-coated separator shows a strong peak at 0.69 keV which is associated with fluorine and confirms the presence of a surface coating (Figure S3, Supporting Information).[28] The infrared transmission spectrum of the coated separator includes strong absorption peaks at 1150 and 1204 cm^{-1}, corresponding to symmetrical and asymmetrical C–F stretching, respectively (Figure 1d).[29,30] Weaker absorption peaks at 970, 982, and 1057 cm^{-1} correspond to C–O–C stretching, C–F stretching (in the –CF$_2$–CF(CF$_3$)-group), and

S–O stretching, respectively. A focused ion beam (FIB) was used to cut a trench into the NC-Celgard surface and SEM images revealed the coating to be ≈ 300 nm thick (Figure 1e). Accompanying EDS maps of carbon and fluorine clearly show the boundary between the Celgard base layer and the Nafion coating (Figure 1f). FIB and SEM of NC-Celgard produced by immersion for a week showed a similar coating of 270 nm, indicating ≈ 300 nm is a self-terminating film thickness on Celgard (Figure S4, Supporting Information) with a 5% Nafion dispersion.

Physical properties of the NC-Celgard separator were then measured to better understand the structure and ion diffusion properties. Celgard 3501, cellophane 350P00, Nafion 211, and Nafion 212 separators were also tested for comparison. The measured and calculated parameters of the commercial and modified separators are shown in **Table 1**.

Water uptake and ionic conductivity were measured to qualitatively determine the ability of ions to migrate through each separator. The addition of the Nafion coating significantly lowered the water uptake over 24 h compared to unmodified Celgard

Table 1. Separator Properties.

Separator	Hydroxide Diffusivity [cm² min⁻¹] × 10⁻⁶	Zincate Diffusivity [cm² min⁻¹] × 10⁻⁶	Selectivity	Water Uptake [%]	Thickness [μm]	Conductivity [mS cm⁻¹]
Celgard 3501	6.7 ± 0.6	5.7 ± 0.8	1.2 ± 0.2	72 ± 5	25 ± 1	12 ± 1.2
Cellophane 350P00	17 ± 0.5	2.0 ± 0.8	8.5 ± 3.0	98 ± 3	25 ± 1	14 ± 1.4
Nafion 211 (N211)	51 ± 6	0.50 ± 0.1	100 ± 20	20 ± 4	25.4 ± 1	8.5 ± 0.8
Nafion 212 (N212)	55 ± 12	0.97 ± 0.5	60 ± 30	19 ± 1	50.8 ± 1	14 ± 4
NC-Celgard	2.2 ± 1.4	≤ 0.0001$^{a)}$	≥ 8000	10 ± 3	25 ± 1	1.7 ± 0.2

$^{a)}$No zincate measured after 25 d, value is calculated from the limit of detection.

**ADVANCED
SCIENCE NEWS**

www.advancedsciencenews.com

**ADVANCED
ENERGY
MATERIALS**

www.advenergymat.de

separators, dropping from 72 ± 5 to 10 ± 3 wt%. Additionally, the ionic conductivity was lower for the NC-Celgard separator than for unmodified Celgard (1.7 ± 0.2 and 12 ± 1.2 mS cm^{-1} respectively, Figure S5, Supporting Information), similar to previous measurements by Kim et al.[25] for Nafion 521 film and Celgard 3501 in 6 M KOH (0.8 and 12.8 mS cm^{-1} respectively). This difference is consistent with the lower water uptake, the observed covering of the Celgard pores, and the hydrophobic perfluoroalkyl nature of Nafion. These lower values imply that using the NC-Celgard in a battery at high rates could be difficult without significant overpotentials; however, we show that the hydroxide permeability is not significantly reduced and that practical cells with the NC-Celgard can still be cycled at rates up to 3 mA cm^{-2}. Wettability and hydrophobicity of the Nafion coating was further quantified by contact angle measurements. The contact angle of water on the Celgard 3501 and NC-Celgard separators was measured as $102.9 \pm 2.8°$ and $112.7 \pm 1.5°$ respectively, corresponding to a $\approx$10% increase with the Nafion coating (Table S1, Supporting Information). Additionally, the surface energy parameters for NC-Celgard, Celgard 3501, and commercial cellophane separators were calculated based on their contact angles with water, ethylene glycol, and diiodomethane (Tables S2 and S3, Supporting Information). These values show good agreement with the literature, as discussed in the Supporting Information, and help to explain the assembly processes.

Figure S6 in the Supporting Information shows the schematics of the experimental setup for peel tests and a typical response for each of the NC-Celgard separators. By averaging the force in the plateau region between 40 and 90 s and normalizing to sample width, the peel strength for each of the separators is determined. The as prepared NC-Celgard displayed the highest peel strength of 0.98 ± 0.22 N m^{-1} with the KOH and ZnO-saturated KOH separators measuring at 0.67 ± 0.10 and 0.63 ± 0.10 N m^{-1}, respectively. While the decrease in peel strength after soaking could be due to unequal expansion of the Celgard and Nafion layers as electrolyte fills pores in the separator, no delamination of the coating was observed upon soaking. The presence of zincate does not appear to have a significant effect. This bodes well for the separator to be used in alkaline Zn batteries where the electrolyte

is often saturated or supersaturated with zincate produced by cell cycling and soluble ZnO at the electrode interface.[2]

Next we investigated the diffusion rates of hydroxide and zincate for each of the separators using an H-cell and our previously introduced assay based on anodic stripping voltammetry (**Figure 2**; Figure S7, Supporting Information).[31] While Nafion is known to be a poor conductor of anions due to Donnan exclusion, the hydroxide crossover rate for commercial Nafion 211 and 212 separators was comparable to Celgard and cellophane (Figure 2a and Table 1). The Nafion coating on Celgard decreased the hydroxide diffusion rate as expected, however, the diffusion coefficients for Celgard ($D_{OH} = 6.7 \pm 0.6 \times 10^{-6}$ cm^2 min^{-1}) and NC-Celgard ($D_{OH} = 2.2 \pm 1.4 \times 10^{-6}$ cm^2 min^{-1}) remain relatively close in value. Compared to other cation exchange membranes, Nafion exhibits greater swelling in aqueous media, allowing permeation of hydroxide through the hydrophilic phase of the material, especially at high ionic strength as used here.[25,32–34] However, the benefit of the thin Nafion coating is evident from our zincate screening experiments, where all the commercial separators (including bulk Nafion) show some zincate crossover within 60 min (Figure 2b and Table 1). Conversely, testing on NC-Celgard continued for 25 d without zincate concentration reaching the limit of detection for the method ($\approx 0.024 \times 10^{-3}$ M). Compared to our previous work with an ion-selective ceramic separator,[35] the NC-Celgard is flexible, thin, and does not appreciably increase the cell volume (<1% change in the cells examined here).

To compare the selectivity of the separators, the hydroxide diffusion coefficient was divided by the zincate diffusion coefficient to output a selectivity ratio R_s. The commercial Celgard and cellophane did not exhibit significant selectivity for hydroxide ($R_s = 1.2 \pm 0.2$ and 8.5 ± 3.0, respectively), while the commercial Nafion separators were much more selective with $R_s = 100 \pm 20$ and 60 ± 30 for Nafion 211 and Nafion 212, respectively. The NC-Celgard separator outperforms all the commercial separators by a substantial margin, significantly hindering the diffusion of zincate ions with a selectivity ratio of 8000 or greater, as determined by the limit of detection.

The negatively charged sulfonate groups in the Nafion coating generate electrostatic repulsion forces with both hydroxide
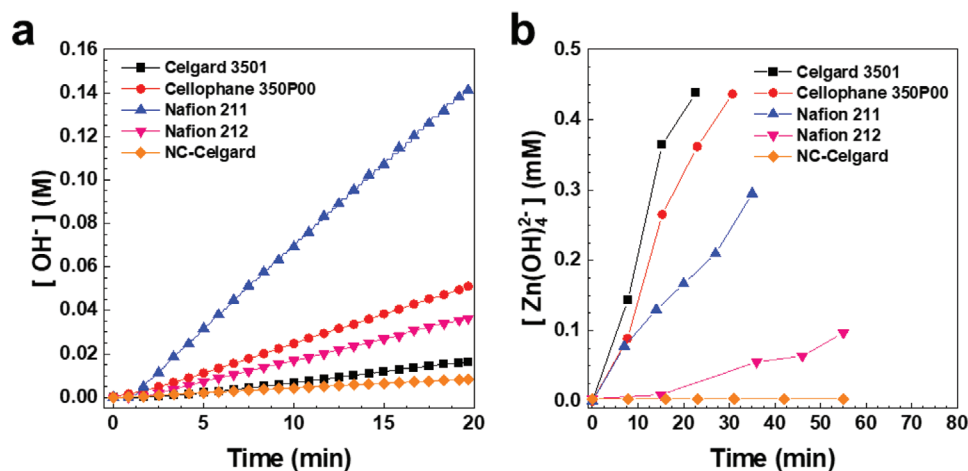

Figure 2. a) Hydroxide concentration (molar) versus time for commercial separators and NC-Celgard. b) Zincate concentration (millimolar) versus time for commercial separators and NC-Celgard. Zn concentration remained below the limit of detection for 25 d of testing the NC-Celgard separator, at which point testing was ceased (data not shown).

and zincate ions. However, charge screening alone is not sufficient to explain the high selectivity of Nafion for hydroxide over zincate. Although zincate is divalent while hydroxide is monovalent, zincate has a threefold larger hydrodynamic radius (0.34 nm, versus 0.11 nm for hydroxide),[36,37] resulting in a more diffuse charge. We believe that size-based exclusion plays an equally important role and that the particularly high selectivity of NC-Celgard stems from its lower wettability compared to bulk Nafion. In hydrated Nafion, the hydrophilic water-containing channels are 1–3.5 nm in diameter.[38–40] While this is greater than the diameter of zincate, the hydration and swelling of Nafion films is known to decrease as film thickness is reduced to the nanoscale (consistent with our water uptake measurements),[41] and the presence of adsorbed ions from the electrolyte could further reduce the channel width.[42] Being only ≈300 nm thick, the Nafion layer in NC-Celgard narrows channels to prevent migration of zincate ions in combination with electrostatic repulsion.

To evaluate the NC-Celgard separator in a more practical context and demonstrate the potential of selective separators in alkaline Zn-based batteries, it was incorporated as a separator in Zn–Ni cells cycled at high capacity utilization of the Zn active material. This system uses energy-dense electrodes that can be manufactured in roll-to-roll processes at scale.[43,44] Specifically, our Zn anodes have a gravimetric capacity of 746 mAh g^{-1} (all capacities are provided per total electrode mass) and an areal capacity of ≈60 mAh cm^{-2} (Table S4, Supporting Information). Such high areal capacities are necessary to make aqueous Zn batteries competitive with Li-ion batteries on a specific energy basis. The NC-Celgard was wrapped around the Zn anode and cells were assembled as shown in Figure S8 in the Supporting Information. Two sets of cells were tested, the first at C/8 (1.5 mA cm^{-2}) based on the cycled capacity and a limit of 20% DOD$_{Zn}$ (hereafter abbreviated 20-DOD-NC and 20-DOD for the cells with NC-Celgard and unmodified Celgard respectively). The other set was cycled with a more aggressive protocol of 50% DOD$_{Zn}$ limit (abbreviated 50-DOD-NC and 50-DOD) at a C/10 (3.0 mA cm^{-2}) rate, again based on target cycled capacity.

In both cases, the Nafion coating imparts a significant improvement in long-term cycling behavior (**Figure 3**a–d).

Figure 3. a) Discharge capacity and discharge energy density, defined relative to volume between and including electrodes (0.605 cm³), for 20-DOD cells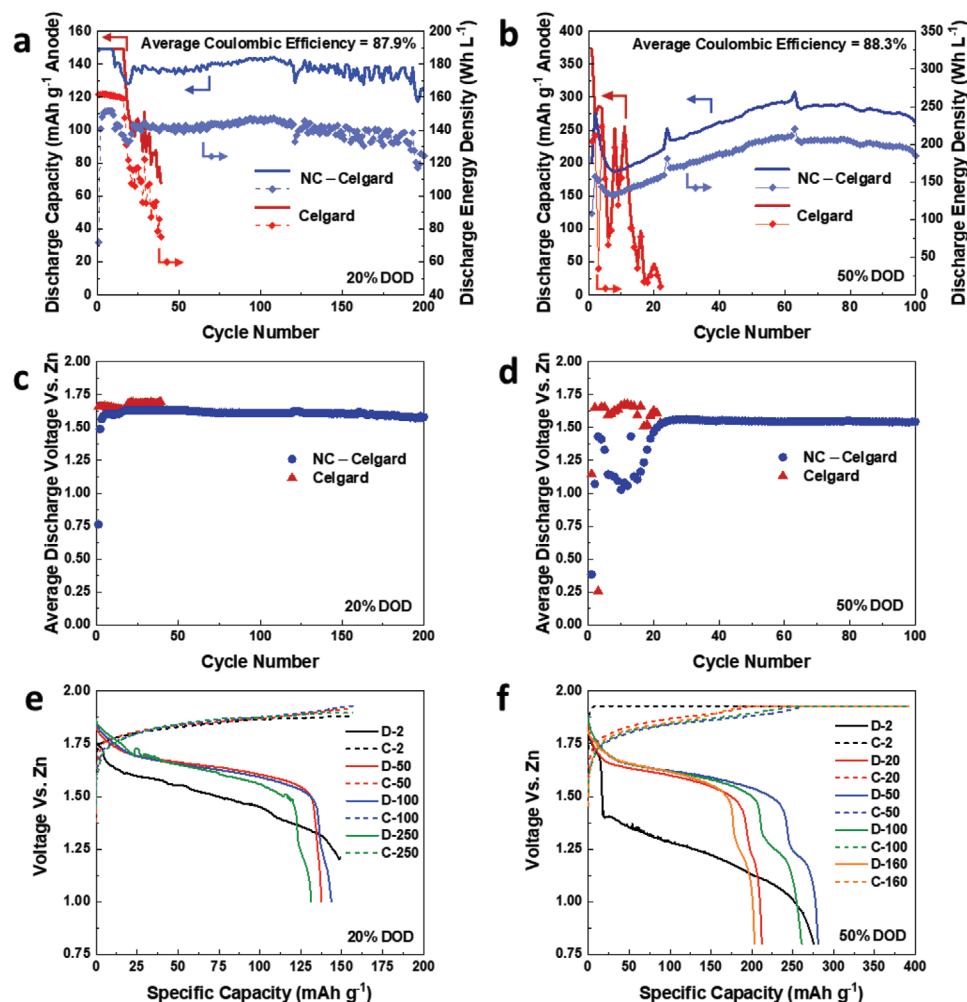. b) Discharge capacity and discharge energy density, defined relative to volume between and including electrodes (0.806 cm³), for 50-DOD cells. c) Average discharge voltage for 20-DOD cells. d) Average discharge voltage for 50-DOD cells. e) 20-DOD-NC cell and f) 50-DOD-NC. Solid lines denote discharge and dashed lines denote charge (following discharge of the same cycle number).

As seen in Figure 3a the inclusion of NC-Celgard drastically increases the cycle lifetime of 20-DOD-NC cells. With only Celgard, the 20-DOD cell begins to fail before reaching 25 cycles but the 20-DOD-NC reaches 200 cycles while maintaining an average DOD_{Zn} of 18.4% (137 mAh g^{-1} anode). The NC-Celgard cell continued to cycle another 350 cycles for a total of 550 cycles with an overall average DOD_{Zn} of 16.3% (122 mAh g^{-1} anode) but suffered from an overall 22.2% capacity fade and drop in average coulombic efficiency from 87.9% to 75.6% from cycle 200 to 550 (Figure S9, Supporting Information). This is considerably better than our recent study examining the positive effect of ZnO-saturated electrolytes on similarly built Zn–Ni cells, where only 259 cycles were achieved in a zincate saturated solution at a 14% DOD_{Zn} limit before massive degradation.[45] The discharge energy density, defined relative to the volume between and including the current collectors,[45–47] follows a similar trend to the capacity, staying above 115 Wh L^{-1} for 200 cycles with an overall average of 140 Wh L^{-1}.

The 50-DOD-NC cell, while not attaining its maximum discharge capacity and energy until cycle 63, still performs impressively (Figure 3b). The cell lasts 100 cycles with an average DOD_{Zn} of 33.9% (253 mAh g^{-1} total anode mass) and discharge energy density of 184 Wh L^{-1}. This is one of the highest combinations of cycle life and specific capacity among recent Zn anode developments, when the latter is normalized to the total mass or area of the anode to compensate for the effect of low active loading as is often employed in experimental electrodes (Table S4, Supporting Information). Like the case of the 20-DOD-NC, the 50-DOD-NC cell continued cycling but decreased in discharge capacity from 261 to 193 mAh g^{-1} and average coulombic efficiency from 88.3% to 78.0% from cycle 100 to 160 (Figure S9b, Supporting Information). As noted in Table S4 (Supporting Information), the performance of 50-DOD-NC is comparable to the 3D Zn sponge anodes reported by Parker et al.[4] and cycled at 40% DOD_{Zn}, but with less complex and time-consuming processing requirements. While not yet proven for high drain applications,[48] the rates examined here demonstrate NC-Celgard is suitable for Zn-batteries for grid-based applications which commonly utilize 3–11 h of discharge time.

For both the 20-DOD-NC and 50-DOD-NC cells, the Nafion coating stabilizes the voltage behavior and prevents shorting from Zn growths that caused sudden failure of the controls (Figure 3c,d). The voltage in the 50-DOD-NC is initially lower but increases gradually for most of its lifetime. The discharge profiles of 20-DOD-NC and 50-DOD-NC remain consistent over the cell lifetime apart from the shortening of the main plateau as the capacity fades, with a steep slope toward the end of discharge and no spikes, even close to failure (Figure 3e,f). This suggests that the Nafion coating confines zincate near the anode surface, where it supersaturates and precipitates more readily rather than diffusing into bulk solution. The ability of a 50-DOD-NC cell to hold a stable open circuit potential after cycling demonstrates that the anode and cathode have not shorted, demonstrating that dendrite growth through the NC-Celgard is not responsible for cell failure (Figure S10a, Supporting Information). Ultimately we believe 20-DOD-NC and 50-DOD-NC cells lose capacity due to detrimental shape change and passivation (Figure S10b, Supporting Information), indi-

cating that additional architectural or chemical modification will likely be needed for further extension of cycle life in high DOD Zn selective separator wrapped cells.

3. Conclusion

In conclusion, we have demonstrated a Nafion-coated microporous polypropylene separator that is effectively impervious to zincate penetration without significant loss of hydroxide transport relative to commercial separators. Furthermore, the separator is thin, flexible, and fabricated by a scalable dip-coating process. In Zn–Ni cells at high Zn utilization, the separator greatly improves cycle life over cells with commercial separators by limiting or slowing active material loss, shape change, and shorting. This shows that this separator is applicable to other secondary alkaline zinc systems that face the same fundamental challenges, including Zn–air, Zn–CuO, or Zn–MnO$_2$. For example, by confining zincate to the anode, such separators could provide an additional benefit to Zn–MnO$_2$ batteries, which have energy densities up to ≈400 Wh L^{-1} and costs potentially below $50 kW h^{-1} when manufactured at scale, but poor cycle life (<100) even with state-of-the-art cathodes and low Zn utilization (≤15%) due to the tendency of zincate to form inactive compounds with the cathode.[47] Eliminating this problem will help zinc battery technology reach reversible energy densities competitive with lithium-ion while offering safer, less expensive materials.

4. Experimental Section

Separator Fabrication: Commercially available Celgard 3501 was submerged in Nafion D-521 dispersion (5% w/w in water and 1-propanol, Alfa Aesar) for 20 h. It was then removed from the solution and hung to dry in air. Excess solution that beaded at the bottom of the separator was removed by dabbing the edge on an absorbent cloth. Both sides of the separator are coated resulting in a ≈300 nm coating on each side.

Hydroxide Diffusion: Hydroxide diffusion was measured using a high-density polyethylene two-chamber diffusion cell (Figure S7, Supporting Information) and an Orion VersaStar Pro pH meter. The feed side of the diffusion cell contained 8.5 M KOH while the draw side contained deionized water. The pH of the draw solution was sampled every 5 s and a diffusion coefficient was calculated using Equation (1)

$$D_X = \frac{V_D \tau}{At} \ln\left(\frac{C_F}{C_F - C_D}\right) \tag{1}$$

where D_{OH} (X = OH) is the diffusion coefficient for hydroxide, V_D is the volume of the draw solution (30 mL), τ is the thickness of the separator, A is the exposed cross sectional area of the separator (1.17 cm^2), C_F is the concentration of hydroxide in the feed solution (8.5 M), and C_D is the concentration of hydroxide in the draw solution.

Zincate Diffusion: Anodic stripping voltammetry (ASV) was used to measure the rate of zincate diffusion across the separators following previously reported methods.[31,49,50] The working electrode was a glassy carbon electrode, 3 mm in diameter (BASi MF-2012). The counter and reference electrodes were a graphite rod and a Hg/HgO electrode (Pine RREF0038 with 1 M KOH filling solution), respectively. Testing was done in the presence of dissolved oxygen from ambient air, using a Pine WaveDriver 20 potentiostat.

Separators were placed in the same two-chamber diffusion cells used for hydroxide diffusion testing. The draw solution consisted of 8.5 M

KOH with 2.5 ppm Pb, 2.5 ppm Cd, and 5 ppm Bi. The feed solution was 4 wt% ZnO in 8.5 M KOH with 2.5 ppm Pb, 2.5 ppm Cd, and 5 ppm Bi. A 30 s cleaning step at 0.3 V under stirring was followed by a deposition step at −1.75 V, also under stirring. Stirring was then stopped and a 25 s rest step was carried out while applying a −1.75 V potential. Square wave voltammetry was performed from −1.75 to 0.3 V with a 5 mV amplitude, 25 mV pulse, and 0.05 s duration resulting in a scan rate of 100 mV s^{-1}. ASV measurements were done periodically on the draw solution to measure zincate concentration over a period of minutes, hours, or days as necessary. The zincate diffusion coefficient D_{Zn} was calculated similarly using Equation (1), where X = Zn.

Ionic Conductivity: The through-plane ionic conductivities of the separators were measured by potentiostatic electrochemical impedance spectroscopy (PEIS) on a Gamry Interface 5000E potentiostat. Separators were cut into 3/8 inch diameter circles and soaked in 4 M KOH overnight before being placed in a "Swagelok cell" with stainless steel blocking electrodes on either side, built similarly to the cell used by Hudak.[51] A frequency range of 1 MHz to 1000 Hz was used with a sinusoidal amplitude of 5 mV from open-circuit potential at room temperature. The resistance of the separator was determined by finding the intercept with the real axis on the Nyquist plot. Ionic conductivity was calculated using Equation (2)

$$\sigma = \frac{\tau}{R_b A} \quad (2)$$

where τ is the thickness of the separator, R_b is the bulk resistance, and A is the cross-sectional area (0.7123 cm^2).

Water Uptake: Separators were placed in deionized water for 24 h to allow for equilibration. Excess water was removed from the surface of the separator and the separators were subsequently weighed. Next, the separators were dried for 24 h in a vacuum oven at 30 °C to obtain the dry weight. The water uptake percentage for each separator was calculated using Equation (3)

$$Water\ Uptake\ (\%) = \frac{m_w - m_d}{m_d} \times 100 \quad (3)$$

where m_w and m_d are the wet and dry separator mass, respectively.

Battery Construction and Testing: For Zn–Ni cell testing, NC-Celgard was prepared at a size of 3 × 1 ¼ inches. Anodes were prepared similarly to the previous work.[45,52–54] 83.1 wt% Zn powder, 9.8 wt% ZnO, 2.2 wt% sodium dodecylbenzenesulfonate (SDBS), and 4.9 wt% polytetrafluoroethylene (PTFE) solids were mixed in a mortar and pestle. Isopropanol was added to produce a malleable putty, which was rolled out to a thickness of ≈0.2 mm, dried at 60 °C, and cut to ¾ x 1 inch. One rectangle of anode material was pressed at 1.9 metric tons onto a Cu mesh current collector. Anodes were subsequently wrapped in the NC-Celgard or unmodified Celgard 3501 (one layer on each side) followed by four layers of cellulose fiber tissue as an electrolyte wicking material. Cathodes were prepared by cutting out rectangles from a commercial sintered NiOOH electrode sheet (Jiangsu Highstar Battery Manufacturing), with an area of ¾ × 1 inch (for 20-DOD cells) or 1 × 1 inch (for 50-DOD cells). The cathode was subsequently wrapped in three layers of cellophane on each side followed by four layers of cellulose fiber tissue. The wrapped anode and cathode were placed in a polypropylene cell case (Flex-A-Top FT9) with ABS shims for compression. The electrolyte was 32 wt% KOH with 4000 ppm tartaric acid and 3000 ppm PEG 400.

Cell cycling was performed on a Maccor Series 4000 multichannel tester. The 20-DOD cells were discharged at a constant current of C/8 (based on cycled capacity) to a cell voltage limit of 1 V or a capacity limit of 20% of the total anode capacity, whichever was reached first. Charging occurred initially at a constant current of C/8 until reaching a capacity limit of 105% of the target DOD (to account for coulombic inefficiencies) or a cell voltage limit of 1.93 V. If the latter was reached first, the cell was held at 1.93 V until the aforementioned capacity limit was reached or the current dropped to 10% of the charge/discharge current of C/8. A 2 min rest occurred between each half-cycle. The 50-DOD cells were cycled similarly but with an anode DOD limit of 50%, lower voltage limit of 0.8 V, and a charge/discharge current of C/10. Cells were cycled until their discharge capacity fell below 50% of the target DOD, at which point they were considered "failed." All capacities are reported per total mass of anode.

Supporting Information

Supporting Information is available from the Wiley Online Library or from the author.

Acknowledgements

Conflict of Interest

The authors declare no conflict of interest.

Data Availability Statement

Research data are not shared.

Keywords

[1] J. F. Parker, J. S. Ko, D. R. Rolison, J. W. Long, *Joule* **2018**, *2*, 2519.

[2] D. E. Turney, J. W. Gallaway, G. G. Yadav, R. Ramirez, M. Nyce, S. Banerjee, Y.-c. K. Chen-Wiegart, J. Wang, M. J. D'Ambrose, S. Kolhekar, J. Huang, X. Wei, *Chem. Mater.* **2017**, *29*, 4819.

[3] S.-B. Lai, M.-I. Jamesh, X. - C. Wu, Y. - L. Dong, J.-H. Wang, M. Gao, J.-F. Liu, X.-M. Sun, *Rare Met.* **2017**, *36*, 381.

[4] J. F. Parker, C. N. Chervin, I. R. Pala, M. Machler, M. F. Burz, J. W. Long, D. R. Rolison, *Science* **2017**, *356*, 415.

[5] M. B. Lim, T. N. Lambert, B. R. Chalamala, *Mater. Sci. Eng., R* **2021**, *143*, 100593.

[6] D. Stock, S. Dongmo, J. Janek, D. Schröder, *ACS Energy Lett.* **2019**, *4*, 1287.

**ADVANCED
SCIENCE NEWS**

www.advancedsciencenews.com

**ADVANCED
ENERGY
MATERIALS**

www.advenergymat.de

[7] N. B. Schorr, D. J. Arnot, A. M. Bruck, J. Duay, M. Kelly, R. L. Habing, L. S. Ricketts, J. A. Vigil, J. W. Gallaway, T. N. Lambert, *ACS Appl. Energy Mater.* **2021**, *4*, 7073.

[8] G. G. Yadav, D. Turney, J. Huang, X. Wei, S. Banerjee, *ACS Energy Lett.* **2019**, *4*, 2144.

[9] W. Fan, F. Liu, Y. Liu, Z. Wu, L. Wang, Y. Zhang, Q. Huang, L. Fu, Y. Wu, *Chem. Commun.* **2020**, *56*, 2039.

[10] C. Zhong, B. Liu, J. Ding, X. Liu, Y. Zhong, Y. Li, C. Sun, X. Han, Y. Deng, N. Zhao, W. Hu, *Nat. Energy* **2020**, *5*, 440.

[11] Z. Zhao, X. Fan, J. Ding, W. Hu, C. Zhong, J. Lu, *ACS Energy Lett.* **2019**, *4*, 2259.

[12] Y. Zhang, Y. Wu, W. You, M. Tian, P.-W. Huang, Y. Zhang, Z. Sun, Y. Ma, T. Hao, N. Liu, *Nano Lett.* **2020**, *20*, 4700.

[13] Y. Wu, Y. Zhang, Y. Ma, J. D. Howe, H. Yang, P. Chen, S. Aluri, N. Liu, *Adv. Energy Mater.* **2018**, *8*, 1802470.

[14] J. Huang, Z. Yang, *ECS Electrochem. Lett.* **2014**, *3*, A116.

[15] Y. Yan, Y. Zhang, Y. Wu, Z. Wang, A. Mathur, H. Yang, P. Chen, S. Nair, N. Liu, *ACS Appl. Energy Mater.* **2018**, *1*, 6345.

[16] D. Stock, S. Dongmo, D. Damtew, M. Stumpp, A. Konovalova, D. Henkensmeier, D. Schlettwein, D. Schröder, *ACS Appl. Energy Mater.* **2018**, *1*, 5579.

[17] A. R. Mainar, L. C. Colmenares, H.-J. Grande, J. A. Blázquez, *Batteries* **2018**, *4*, 46.

[18] M. Chamoun, B. J. Hertzberg, T. Gupta, D. Davies, S. Bhadra, B. Van Tassell, C. Erdonmez, D. A. Steingart, *NPG Asia Mater.* **2015**, *7*, e178.

[19] I. V. Kolesnichenko, D. J. Arnot, M. B. Lim, G. G. Yadav, M. Nyce, J. Huang, S. Banerjee, T. N. Lambert, *ACS Appl. Mater. Interfaces* **2020**, *12*, 50406.

[20] E. L. Dewi, K. Oyaizu, H. Nishide, E. Tsuchida, *J. Power Sources* **2003**, *115*, 149.

[21] H. J. Hwang, W. S. Chi, O. Kwon, J. G. Lee, J. H. Kim, Y.-G. Shul, *ACS Appl. Mater. Interfaces* **2016**, *8*, 26298.

[22] B.-S. Lee, S. Cui, X. Xing, H. Liu, X. Yue, V. Petrova, H.-D. Lim, R. Chen, P. Liu, *ACS Appl. Mater. Interfaces* **2018**, *10*, 38928.

[23] D. Yuan, W. Manalastas Jr., L. Zhang, J. J. Chan, S. Meng, Y. Chen, M. Srinivasan, *ChemSusChem* **2019**, *12*, 4889.

[24] Z. Yuan, X. Liu, W. Xu, Y. Duan, H. Zhang, X. Li, *Nat. Commun.* **2018**, *9*, 3731.

[25] H.-W. Kim, J.-M. Lim, H.-J. Lee, S.-W. Eom, Y. T. Hong, S.-Y. Lee, *J. Mater. Chem. A* **2016**, *4*, 3711.

[26] Y. Li, H. Dai, *Chem. Soc. Rev.* **2014**, *43*, 5257.

[27] M. Ghosh, V. Vijayakumar, B. Anothumakkool, S. Kurungot, *ACS Sustainable Chem. Eng.* **2020**, *8*, 5040.

[28] Periodic Table of Elements and X-ray Energies, http://bruker.com/hhxrf (accessed: June 2021).

[29] C. Heitner-Wirguin, *Polymer* **1979**, *20*, 371.

[30] Z. Liang, W. Chen, J. Liu, S. Wang, Z. Zhou, W. Li, G. Sun, Q. Xin, *J. Membr. Sci.* **2004**, *233*, 39.

[31] J. Duay, T. N. Lambert, R. Aidun, *Electroanalysis* **2017**, *29*, 2261.

[32] A. Münchinger, K.-D. Kreuer, *J. Membr. Sci.* **2019**, *592*, 117372.

[33] M. T. Tsehaye, F. Alloin, C. Iojoiu, R. A. Tufa, D. Aili, P. Fischer, S. Velizarov, *J. Power Sources* **2020**, *475*, 228689.

[34] Z. Yuan, H. Zhang, X. Li, *Chem. Commun.* **2018**, *54*, 7570.

[35] J. Duay, *J. Power Sources* **2018**, *395*, 430.

[36] Y. Marcus, *J. Chem. Phys.* **2012**, *137*, 154501.

[37] E. J. Pessine, S. M. L. Agostinho, H. C. Chagas, *Can. J. Chem.* **1986**, *64*, 523.

[38] K. A. Mauritz, R. B. Moore, *Chem. Rev.* **2004**, *104*, 4535.

[39] Q. Duan, H. Wang, J. Benziger, *J. Membr. Sci.* **2012**, *392–393*, 88.

[40] K. Schmidt-Rohr, Q. Chen, *Nat. Mater.* **2008**, *7*, 75.

[41] S. A. Eastman, S. Kim, K. A. Page, B. W. Rowe, S. Kang, C. L. Soles, K. G. Yager, *Macromolecules* **2012**, *45*, 7920.

[42] H. Zhang, J. Pan, X. He, M. Pan, *J. Appl. Polym. Sci.* **2008**, *107*, 3306.

[43] N. Ingale, T. Sholklapper, *U.S. Patent Application 20150311503*, **2015**.

[44] M. Menard, D. Kaplin, R. Cammarata, *U.S. Patent Application 20190157726*, **2019**.

[45] M. B. Lim, T. N. Lambert, E. I. Ruiz, *J. Electrochem. Soc.* **2020**, *167*, 060508.

[46] G. G. Yadav, J. W. Gallaway, D. E. Turney, M. Nyce, J. Huang, X. Wei, S. Banerjee, *Nat. Commun.* **2017**, *8*, 14424.

[47] G. G. Yadav, X. Wei, J. Huang, J. W. Gallaway, D. E. Turney, M. Nyce, J. Secor, S. Banerjee, *J. Mater. Chem. A* **2017**, *5*, 15845.

[48] L. Yin, J. Scharf, J. Ma, J.-M. Doux, C. Redquest, V. Le, Y. Yijie, J. Ortega, X. Wei, J. Wang, Y. S. Meng, *Joule* **2021**, *5*, 228.

[49] J. Duay, J. E. Ortiz-Santiago, T. N. Lambert, *Electroanalysis* **2017**, *29*, 2685.

[50] D. J. Arnot, T. N. Lambert, *Electroanalysis* **2021**, *33*, 797.

[51] N. S. Hudak, L. J. Small, H. D. Pratt, T. M. Anderson, *J. Electrochem. Soc.* **2015**, *162*, A2188.

[52] J. Duay, M. Kelly, T. N. Lambert, *J. Power Sources* **2018**, *395*, 430.

[53] J. Duay, T. N. Lambert, M. Kelly, I. Pineda-Dominguez, *J. Electrochem. Soc.* **2019**, *166*, A687.

[54] M. Kelly, J. Duay, T. N. Lambert, R. Aidun, *J. Electrochem. Soc.* **2017**, *164*, A3684.